Finite element simulation for damage detection of surface rust in steel rebars using elastic waves

Qixiang Tang, Tzuyang Yu

Qixiang Tang, Tzuyang Yu, "Finite element simulation for damage detection of surface rust in steel rebars using elastic waves," Proc. SPIE 9804, Nondestructive Characterization and Monitoring of Advanced Materials, Aerospace, and Civil Infrastructure 2016, 980426 (22 April 2016); doi: 10.1117/12.2219265

SPIE.

Event: SPIE Smart Structures and Materials + Nondestructive Evaluation and Health Monitoring, 2016, Las Vegas, Nevada, United States

Finite Element Simulation for Damage Detection of Surface Rust in Steel Rebars using Elastic Waves

Qixiang Tang and Tzuyang Yu

Department of Civil and Environmental Engineering
University of Massachusetts Lowell
One University Avenue, Lowell, MA 01854, U.S.A.

ABSTRACT

Steel rebar corrosion reduces the integrity and service life of reinforced concrete (RC) structures and causes their gradual and sudden failures. Early stage detection of steel rebar corrosion can improve the efficiency of routine maintenance and prevent sudden failures from happening. In this paper, detecting the presence of surface rust in steel rebars is investigated by the finite element method (FEM) using surface-generated elastic waves. Simulated wave propagation mimics the sensing scheme of a fiber optic acoustic generator mounted on the surface of steel rebars. Formation of surface rust in steel rebars is modeled by changing material's property at local elements. In this paper, various locations of a fiber optic acoustic transducer and a receiver were considered. Megahertz elastic waves were used and different sizes of surface rust were applied. Transient responses of surface displacement and pressure were studied. It is found that surface rust is most detectable when the rust location is between the transducer and the receiver. Displacement response of intact steel rebar is needed in order to obtain background-subtracted response with a better signal-to-noise ratio. When the size of surface rust increases, reduced amplitude in displacement was obtained by the receiver.

Keywords: Finite element method (FEM), damage detection, rebar corrosion

1. INTRODUCTION

Damage detection of civil infrastructure using elastic waves has been reported in various applications. Methods such as impact-echo method[1,2] utilizing bulk waves (compressive and shear wave) are proved to be useful for detecting flaws inside concrete specimen. Using guided wave method is also a popular non-destructive testing method. Guided wave has high sensitivity to most types of damage and high efficiency in detecting small and subsurface defects.[3]

Among different types of elastic waves, surface waves (i.e., Rayleigh waves) are most frequently used for the detection of surface defect.[4,5] Cook and Berthelot[6] used root mean square of scattered Rayleigh waves' amplitude (surface displacement) for the detection of small surface fatigue cracks. Resch and Nelson[7] proposed a model predicting the relationship between crack size and the surface displacement of the reflected echo from a crack. Finite element method (FEM) are widely used on simulating surface wave propagation. However, it is quite challenging to simulate surface waves with high frequency (e.g., ultrasonic wave) since the element size needs to be small enough to represent the wavelength. Thus, the solution time increases incredibly. To improve the computational efficiency of simulations,different FE modeling strategies on absorbing regions have been developed.[8,9]

Instead of commonly used elastic wave generator (e.g., falling steel sphere) or transducer, Zhou *et al.*[10 11] suggested that fiber optic photoacoustic ultrasound generator could be used as an elastic wave generator. Nevertheless, an efficient sensing scheme is required.

This paper aims at developing a corrosion sensing scheme for small transducers and receivers as small as fiber optic sensors. Displacement response is used for detecting, locating, and quantifying surface rust in rebar structures. FEM is applied in building numerical rebar models and simulating wave propagation in rebar models.

Further author information: (Send correspondence to T. Yu)
E-mail: tzuyang_yu@UML.EDU, Telephone: 1 978 934 2288

Nondestructive Characterization and Monitoring of Advanced Materials, Aerospace, and Civil Infrastructure 2016, edited by Tzuyang Yu, Andrew L. Gyekenyesi, Peter J. Shull, H. Felix Wu,
Proc. of SPIE Vol. 9804, 980426 · © 2016 SPIE · CCC code: 0277-786X/16/$18 · doi: 10.1117/12.2219265

Table 1. Material properties

	Steel	Rust
Density	7.85×10^{-9} ton/mm^3	2.61×10^{-9} ton/mm^3
Young's Modulus	210×10^3 MPa	500 MPa
Poisson's ratio	0.3	0.3

A commercial FE software package ABAQUS® (by Dassault Systems) is chosen for its wide applications in explicit analysis.

Four receiver locations are distributed on the model, collecting transient displacement response. In this development, net displacement response and an indicator are combined to i) detect corrosion, ii) locate corrosion, and iii) quantify corrosion.

In this paper, FE modeling of intact and corroded rebar models is first described. Design of FE models and the characterization of artificial corrosion are provided. A corrosion detection scheme is proposed based on the maximum net displacement response at locations of the fiber optic photoacoustic receiver. Finally, research findings are discussed.

2. FINITE ELEMENT MODELING

To study the wave propagation in intact and corroded rebars, FE models were designed and used. An intact model was created first with 705600 linear hexahedral elements of type C3D8R, based on the geometry and material property of a standard number four steel rebar. By introducing surface rust (corrosion) to the intact model, 14 corroded models were made. In each model, the two ends are fixed and a sinusoidal pulse was applied at mid-span. Displacement responses at four locations were collected and analyzed. FE modeling details are described in the following.

2.1 Material Property and Geometry

2.1.1 Intact Rod Models

The intact model was made of steel, property of which is provided in Table 1. An intact rod model was designed base on a standard No.4 steel rebar. Complicated, detailed features such as ribs and lugs of the rebar were not included. In this research, the simplified rod model was a 50 mm (1.97 in) cylinder with a diameter of 12.7 mm (0.5 in), as shown in Figs. 1.

2.1.2 Corroded Rod Models

Introduction of an artificial corrosion was achieved by changing the material property at corroded region from steel to rust. (Rust's property is also provided in Table.1.) Each corroded model only contained one corroded region. To characterize a corroded region, four attributes were defined: location L^j, depth l_z, width l_θ, and thickness l_ρ. These attributes are further explained in the following.(Fig.2 illustrates these attributes).

- Corroded region location, L^j $(j = 1, 2)$ - As shown in Fig. 2, L^1 is a corroded region on the top of the rod; it is 5 mm away from the mid-span. L^2 is located at mid-span. In the cylindrical coordinate system, L^1 and L^2 have 90 degrees of difference on the θ axis.
- Corroded region size, $l_\rho \in [0, 2]$ (mm), $l_\theta \in [0, 10, 20, 30, 40]$ $(^\circ)$ and $l_z \in [0, 1, 2, 3, 4]$ (mm) - Damage size was quantified by three parameters: thickness, depth and width of the corroded region. The subscript indicates the axis on which the dimension describes. For example, l_z describes length of a corroded region on z-axis. (Note that the thickness l_ρ of all corroded regions were fixed to $2mm$.)

Fourteen models with different combinations of above attributes were made and listed in Table 2.

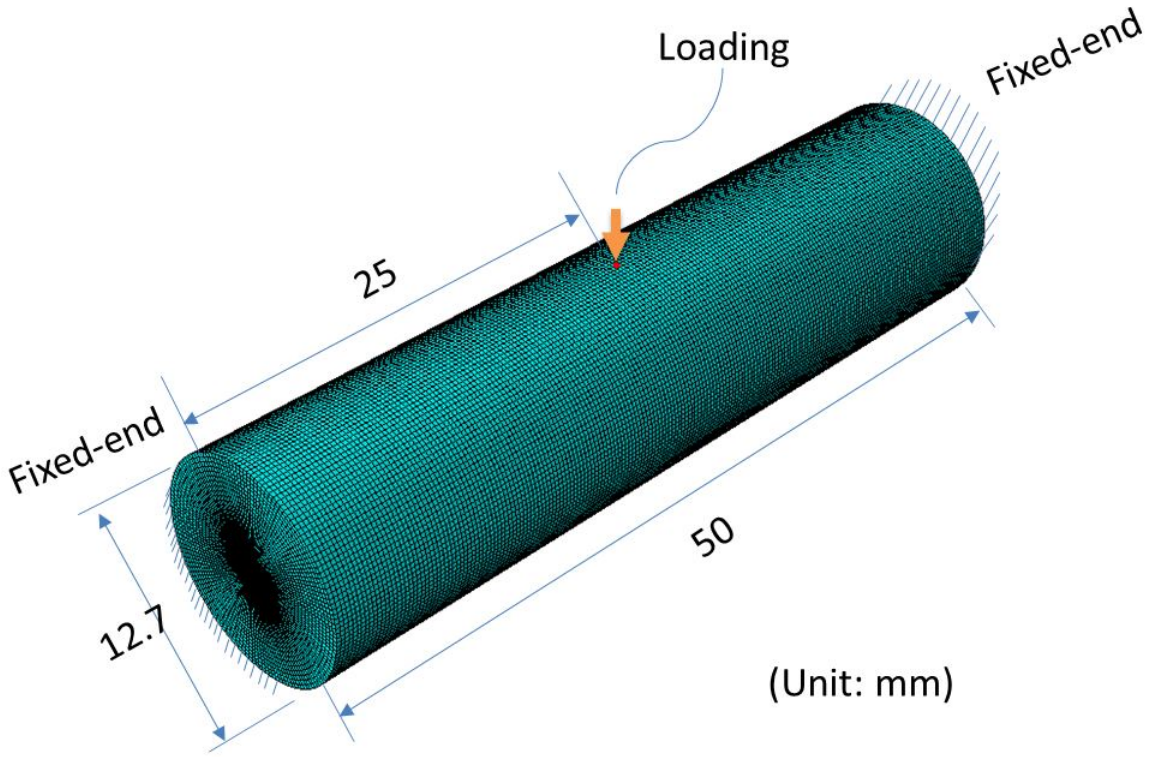

Figure 1. Simplified rod model

2.2 Boundary Conditions and Loading

Both ends of each model were fixed. In addition, at each end, 10 mm (0.39 in) of absorbing regions were applied, as shown in Fig. 3. These regions were created with absorbing layers using increasing damping (ALID),[12] and they function as non-reflecting boundaries. Elastic waves were gradually damped out when they propagate into an absorbing region. The material's property in these regions is similar to that of the core apart from additional damping. Each of these regions contains 10 layers. The damping value of these layers linearly increases from the interface between the core and absorbing regions, to the fixed end.

Four locations of a fiber optic photoacoustic receiver were considered, defined as $A_i (i = 0, 1, 2 \text{ and } 3)$, as shown in Fig. 4. A transducer is placed at A_0, generating a sinusoidal pulse (Fig. 5). Transient displacement responses, normal to the model's surface, at four considered locations (A_0, A_1, A_2 and A_3) were collected. As a result, four transducer-receiver pairs are studied.

2.3 Net Displacement Response

The displacement responses can be affected by the introduction of artificial corrosion. The differential displacement at A_i caused by the corrosion locating at L^j is defined as the net displacement response δu_i^j. It can be calculated by:

$$\delta u_i^j = u_i^j - u_i^{int} \tag{1}$$

where u_i^j = displacement response of a corroded rod model at A_i, u_i^{int}= displacement response of intact model at A_i and δu_i^j= net displacement response of the corroded rod at Ai. To determine which pair is the best sensing

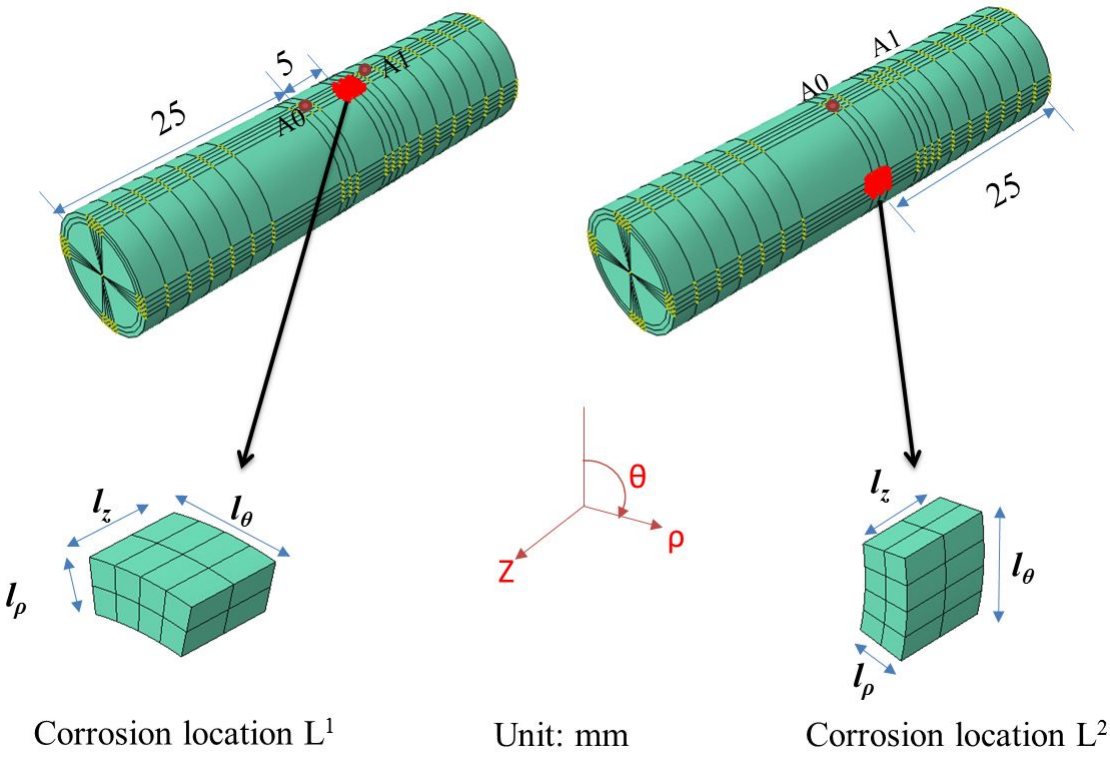

Figure 2. Two considered corrosion locations

scheme for detecting corrosion/surface rust, a characteristic parameter named indicator, I_i^j, was proposed and defined as the normalized maximum net displacement response at A_i.

$$I_i^j = \left| \frac{(\delta u_i^j)_{max}}{(u_i^{int})_{max}} \right| \times 100\ \% \tag{2}$$

in which $(u_i^{int})_{max}$ is the maximum displacement response of a intact rod model obtained at A_i.

Displacement response at each location for all corrosion cases was obtained from FE simulations. Net displacement response was calculated using Eq. (1).

3. SIMULATION RESULTS

3.1 Net Displacement Response

As an example, Figs. 6 and 7 show net displacement responses at all four locations for case #2 and #9. In order to evaluate the effectiveness of locations A_i in terms of detecting corrosion, maximum net displacement responses from cases #2 and #9 are summarized into Table 3. Note that the corroded region of cases #2 and #9 has identical sizes.

3.2 Indicator I_i^j

Similar to the net displacement response, indicator I_i^j is calculated using Eq. (2). Table 4 lists the value of I_i^j for cases #2 and #9.

Table 2. Considered corrosion cases

Case #	L^j	l_ρ (mm)	l_θ $(^\circ)$	l_z (mm)
1	L^1	2	20	1
2	L^1	2	20	2
3	L^1	2	20	3
4	L^1	2	20	4
5	L^1	2	10	2
6	L^1	2	30	2
7	L^1	2	40	2
8	L^2	2	20	1
9	L^2	2	20	2
10	L^2	2	20	3
11	L^2	2	20	4
12	L^2	2	10	2
13	L^2	2	30	2
14	L^2	2	40	2

Table 3. Maximum net displacement response $(\delta u_i^j)_{max}$

Transducer	Receiver	case #2 ($\times 10^{-6}$ mm)	case #9 ($\times 10^{-6}$ mm)
A_0	A_0	0.64	2.09
A_0	A_1	**3.05**	1.33
A_0	A_2	0.59	**3.09**
A_0	A_3	0.94	0.97

Table 4. Indicator I_i^j of case #2 and #9

Transducer	Receiver	case #2 (%)	case #9 (%)
A_0	A_0	0.8	4.93
A_0	A_1	**36.45**	**15.92**
A_0	A_2	3.15	**16.14**
A_0	A_3	8.74	9.01

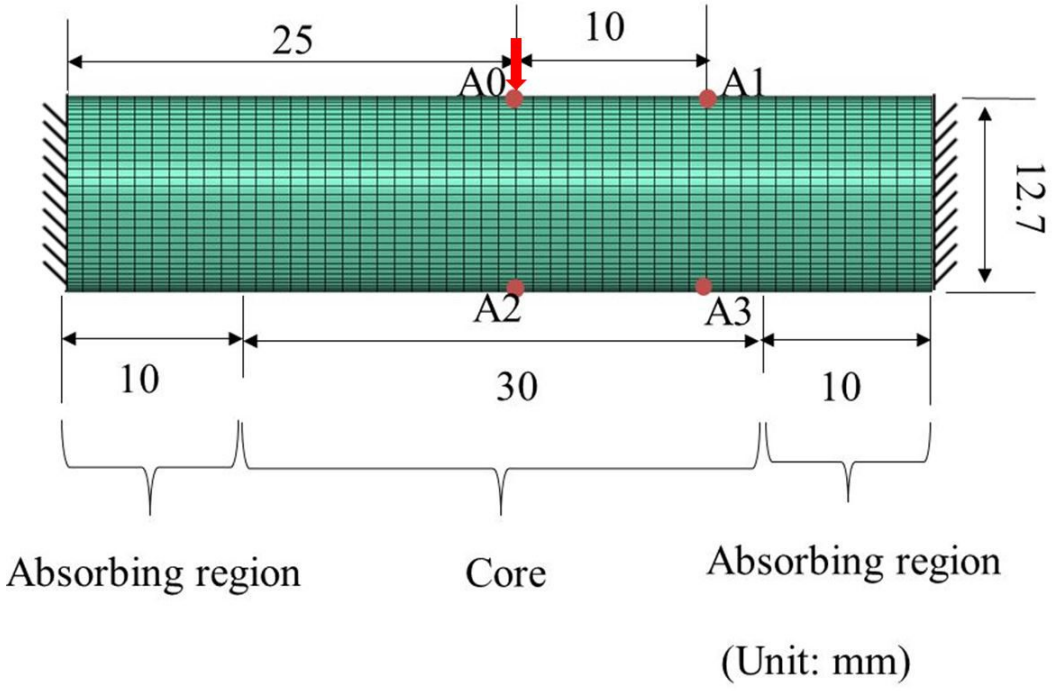

Figure 3. Absorbing Regions

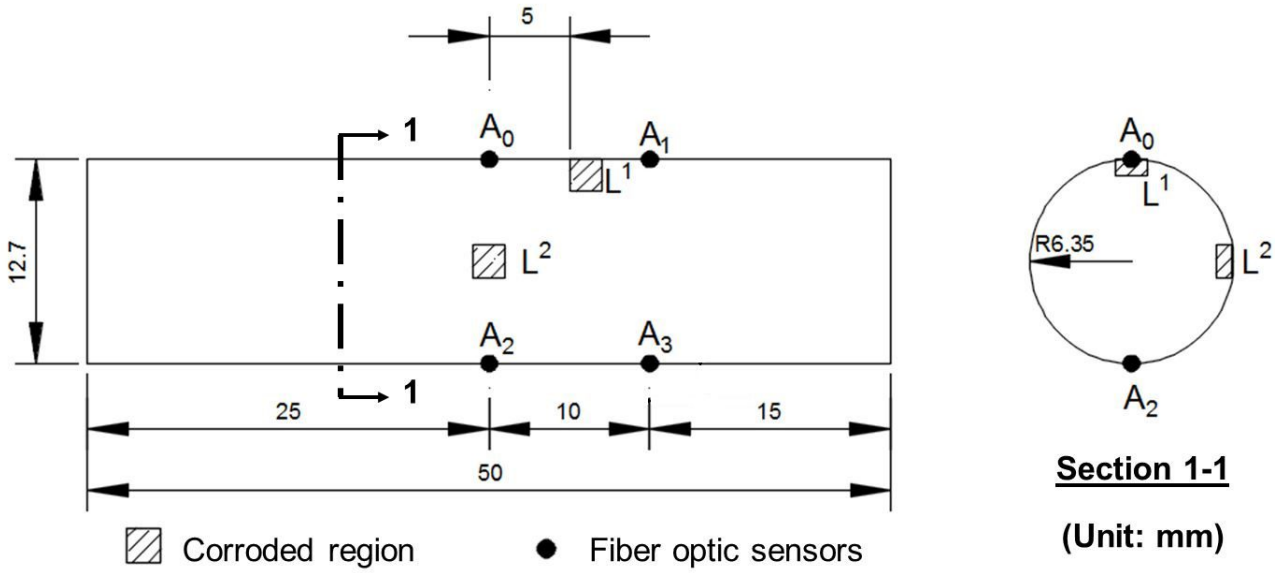

Figure 4. Locations of the fiber optic photoacoustic receiver

3.3 Corrosion Detection

Evaluation of receiver locations for corrosion detection is achieved by checking the maximum net displacement response and indicator I_i^j.

- Corrosion detection – Indicator I_i^j at A_1 can be used to detect the presence of corrosion since it has high value of the indicator in cases #2 and #9. From the definition of indicator I_i^j, any non-zero value of I_i^j

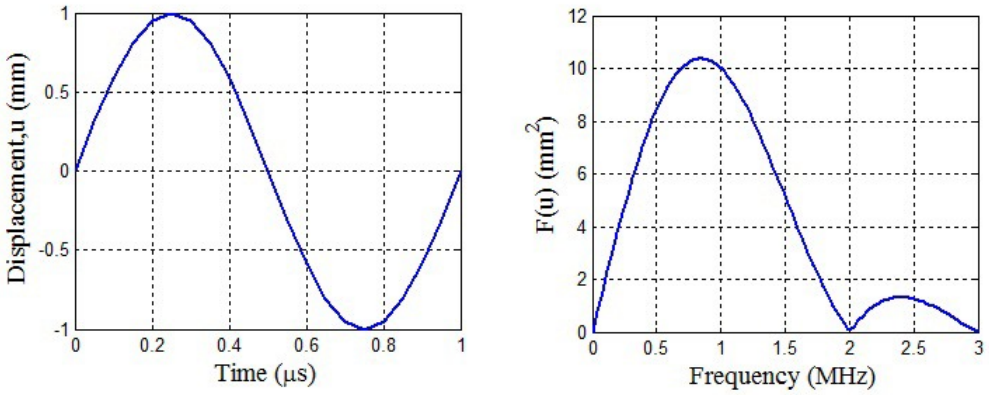

Figure 5. Input function

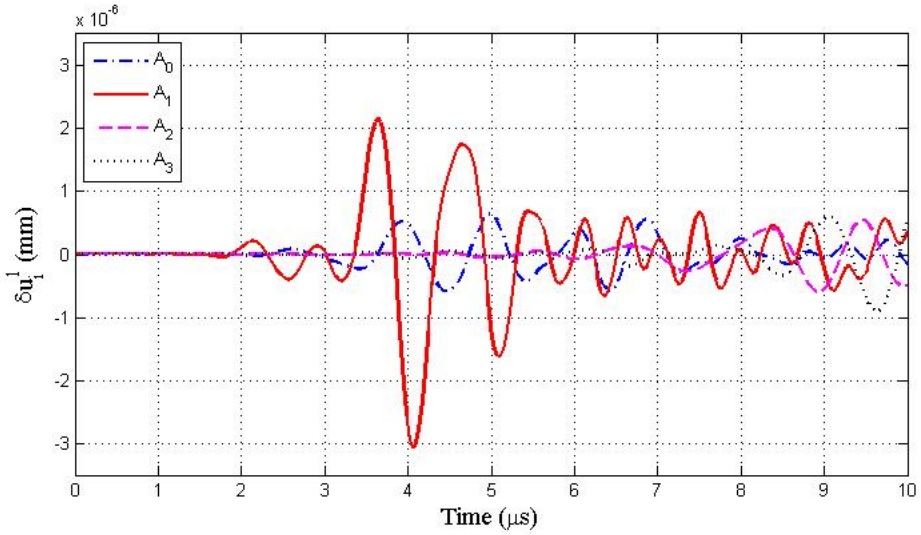

Figure 6. Net Displacement of case #2

suggests the appearance of corrosion. However, the sensitivity of considered receivers changes for same levels of corrosion. In Table 4, A_1 always has greater values in both cases #2 and #9.

- Corrosion location – For considered corrosion locations (L^j), the greatest net displacement response $(\delta u_i^j)_{max}$ at A_1 predicts corrosion located at L^1; the greatest $(\delta u_i^j)_{max}$ at A_0 or A_2 predicts corrosion location at L^2. It is found that when the corrosion is between a receiver and the transducer, $(\delta u_i^j)_{max}$ of this receiver have the greatest value against the values of other receivers. For example, in case #2 and with a $(u_i^j)_{max}$ value at A_1, corrosion is predicted to be located between A_1 (receiver) and A_0 (transducer). From Table 3, value of A_1 is much greater than any other locations. Similarly, in case #9, corrosion locates between A_2 (receiver) and A_0 (transducer). (A_0 is also a receiver in this case.) In Table 3, $(\delta u_i^j)_{max}$ of both A_0 and A_2 are greater than other receivers. In frequency domain, similar patter can be also observed. Frequency response was disturbed more when corrosion is between the transducer and receiver, than the case that corrosion is not between. As an example, Fig.8 shows the frequency response at A_2 for both case #2 and #9. While frequency response at A_2 in case #2 is almost overlapped with the one in intact model, frequency response in case #9 (corrosion is between the transducer and receiver) is distorted from frequency response of the intact model (e.g.,frequency peak at 0.87 MHz becomes narrower in case #9).
- Corroded region size – To determine the size of corroded region, an empirical equation is developed.

$$l_{\theta,orz} = a \times exp[b \times (\delta u_i^j)_{max}] \tag{3}$$

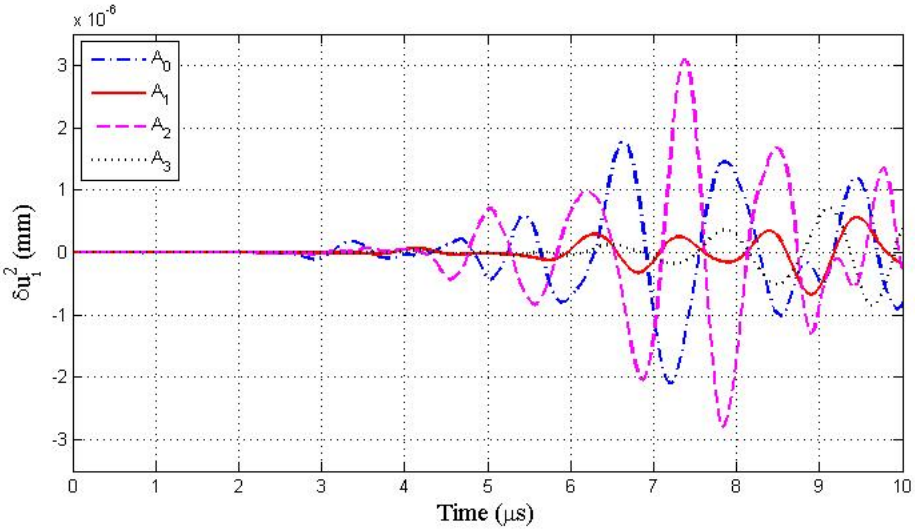

Figure 7. Net Displacement of case #9

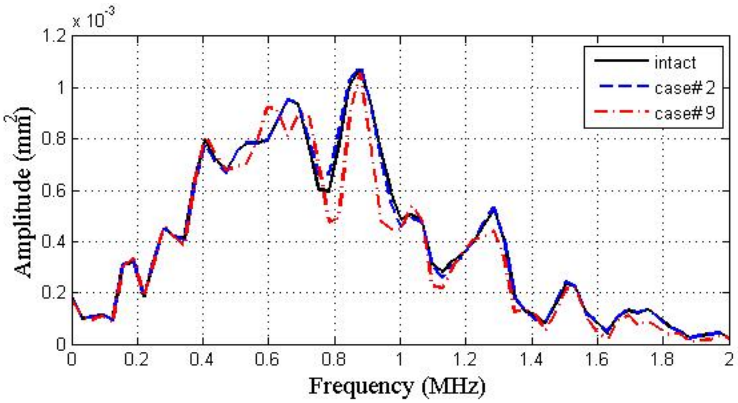

Figure 8. Frequency responses at A_2

Table 5 lists the values of coefficients used in Eq. 3, as well as their R^2 evaluation.

Table 5. Coefficients of empirical equations for quantifying corrosion

L^j		a	b	R^2
L^1	l_θ	3.335	2.90×10^5	0.97
	l_z	0.106	4.98×10^5	0.96
L^2	l_θ	0.385	3.87×10^5	0.96
	l_z	3.4	2.23×10^5	0.97

4. SUMMARY AND DISCUSSION

From the FE simulations, the appearance of corrosion causes more differential displacement at A_1 (corrosion at L^1 and L^2) and A_2 (corrosion at L_2) than at other locations. This result suggests that indicator I_i^j becomes greatest (most sensitive) when the corroded region is located between the transducer and the receiver. Once the corrosion is detected, maximum net displacement response (δu_i^j) can be used to calculate the dimension of the corroded region. The proposed sensing scheme is summarized and discussed in the following.

- Corrosion detection - The best sensing scheme to detect corrosion is 'transducer - corrosion - receiver'. Therefore, it's good to put receivers at both A_1 and A_2, such that corrosions between A_0 and A_1, or A_0 and A_2 can be detected. However, if only one receiver is allowed, location A_1 is the best option since indicator I_i^j is sensitive to both L^1 and L^2. (I_i^j is greater than 15 for both L^1 and L^2.)
- Corrosion size - Using predetermined relationship (Eq.(3)) between corrosion dimension (l_θ or l_z) and maximum net displacement response $\delta u_{i\,max}^j$, corrosion size can be estimated.

5. CONCLUSION

In this paper, a sensing scheme utilizing the maximum net displacement response (δu_i^j) and indicator I_i^j is reported for detecting, locating and quantifying corroded region in simplified rod models. This sensing scheme can be used as guidance for the optimal design of surface rust detecting using small sensors (e.g., fiber optic photoacoustic sensors) on rod structures. It is believed that this sensing scheme has a great potential to be combined with fiber optic photoacoustic sensors[10] and used for evaluating and monitoring of rebar structures in practice.

6. ACKNOWLEDGEMENT

The authors want to express their gratitude to the partial support from the National Science Foundation (NSF), the Civil, Mechanical and Manufacturing Innovation (CMMI) Division, through a grant CMMI #1401369 (PI: Prof. X. Wang, UMass Lowell) to this research.

REFERENCES

[1] Sansalone, M. and Carino, N. J., "The transient impact response of plates containing disk-shaped flaws," National Bureau of Standards Journal of Research Nov./Dec., 369–381 (1987).
[2] Sansalone, M. and Carino, N. J., "The transient impact response of thick circular plates," National Bureau of Standards Journal of Research Nov./Dec., 355–367 (1987).
[3] Rose, J. L., "A baseline and vision of ultrasonic guided wave inspection potential," J. Pressure Vessel Technol. 124., 273–282 (2002).
[4] Worlton, D. C., "Ultrasonic testing with lamb waves," NonDestructive Testing 15, 218–222 (1957).
[5] Rose, J. L., "A vision of ultrasonic guided wave inspection potential," Proceedings of the 7th ASME NDE Topical Conference 20, 1–5 (2001).
[6] Cook, D. and Berthelot, Y., "Detection of small surface-breaking fatigue cracks in steel using scattering of rayleigh waves," NDT E International 34, 483–492 (2001).
[7] Resch, M. T. and Nelson, D. V., "An ultrasonic method for measurement of size and opening behavior of small fatigue cracks," Small-crack test methods. ASTM International, , 169–196 (1992).
[8] Liu, G. R. and Quek, S. S., "A non-reflecting boundary for analyzing wave propagation using the finite element method," Fn. Elem. in Anal. Des. 39, 403–417 (2003).
[9] Drozdz, M., Moreau, L., Castaings, M., Lowe, M. J. S., and Cawley, P., "Efficient numerical modelling of absorbing regions for boundaries of guided waves problems," J. Acoust. Soc. Am. 115., 126133 (2006).
[10] Zou, X., Schmitt, T., Perloff, D., Wu, N., Yu, T., and Wang, X., "Nondestructive corrosion detection using fiber optic photoacoustic ultrasound generator," Measurement 62, 74–80 (2015).
[11] Wu, N., Zou, X., Zhou, J., and Wang, X., "Fiber optic ultrasound transmitters and their applications," Measurement 79, 164–171 (2016).
[12] Drozdz, M., "Efficient finite elemnet modeling of ultrasound waves in elastic media," Diss. University of London (2008).